Behavior of a Deep Excavation and Damages on Adjacent Buildings: a Case Study in Vietnam

Quoc Thien Huynh[1] · Van Qui Lai[2,3] · Tirawat Boonyatee[4] ·
Suraparb Keawsawasvong[5]

Abstract

This paper investigates the behavior of deep excavations and damages on adjacent buildings based on an excavation in a thick sand layer in Vietnam. Firstly, measured horizontal displacements of diaphragm walls were used to calibrate soil stiffness parameters for finite element analysis (FEA). Then, the behavior of diaphragm walls, groundwater, ground surface deformation, and an adjacent building was analyzed. The analysis results and damages observed in the field were used to review the validity of the criteria for evaluating the damage potential of excavation to adjacent buildings. It can be concluded from the study that the damage potential of adjacent buildings as evaluated from FEA through the strain state chart proposed by Boscardin and Cording (1989) or the damage potential index (DPI) proposed by Schuster et al. (2009) is fairly accurate with field observations.

Keywords Deep excavation · Damage potential criteria · Thick sand layer

1 Introduction

Construction of deep basements in narrow spaces is inevitable in urbanized areas. The design and construction of deep excavations under such situations require great attention to ensure stability and to minimize the impact on adjacent buildings. During the

✉ Van Qui Lai
lvqui@hcmut.edu.vn

Quoc Thien Huynh
huynhquocthien@duytan.edu.vn

Tirawat Boonyatee
dr.tirawat@gmail.com

Suraparb Keawsawasvong
suraparb@hotmail.com

Extended author information available on the last page of the article

initial design and preparation stage, it is convenient to assess the damage potential of adjacent buildings by some simple rules. For this purpose, the damage potentials may be evaluated from the angular distortion β and the tensile strain ε_L (Skempton and MacDonald 1956; Burland et al. 1978; Boscardin and Cording 1989; Son and Cording 2005). Schuster et al. (2009) performed a regression analysis on collected field observations and proposed simple equations for predicting the β and ε_L values. Sabzi and Fakher (2015) applied the criteria proposed by Schuster et al. (2009) to a shallow excavation next to a low-rise building with inclined struts. Halim and Wong (2011) discussed the damage assessments of adjacent buildings by considering the influence zone of excavations and current structural conditions from visual inspection surveys. In general, these studies considered the performance of retaining wall, ground surface, and an adjacent building in separate models or only used measured field data to assess damage levels of adjacent buildings. Lin et al. (2016) assumed a simple artificial case study to estimate the damage potential of an adjacent building by employing finite element analysis (FEA).

The objective of this study is to investigate behaviors of deep excavations and damages on adjacent buildings based on both field observations and FEA results. A new approach for evaluating the damage level of the adjacent building is proposed based on deformations obtained from calibrated FEA.

2 A Case Study

2.1 Project Descriptions and Soil Conditions

A deep excavation project, namely Madison, located at 15 Thi Sach street, District 1, Ho Chi Minh City, Vietnam, as shown in Fig. 1, is adopted in the numerical simulation in this study. The project consisted of 17 stories and 3 basements placed in an area of 2360 m². The excavation was 65 m long and 37 m wide. The excavation was carried out by the semi top-down construction method and retained by reinforced concrete diaphragm wall (D-wall) which is 0.8 m thick and 37 m deep. It underwent 4 excavation stages with four-level slabs in conjunction with steel struts. The maximum excavation depth was 15.5 m from the ground level (GL). Figure 2 shows the cross-section, surcharge load, geological conditions, construction sequences, strutting systems, and excavation levels. More details on the excavation sequences can be found in Table 1. Besides, the SPT-N values from four boreholes of the project are shown in Fig. 3.

The ground consists of two sandy and three clayey soil layers. The 3rd layer is a thick medium dense sand layer with SPT-N values ranging from 8 to 25 blows/ft from the depth of 5 to 35 m, respectively. It has a significant influence on the behavior of the retaining system because most excavation works were conducted in this layer. The first two layers (1st and 2nd clay layers) are located at depths of 1.5–4.5 m and 4.5–5.5 m below the ground surface, respectively. The 1st and 2nd layers are very soft clay with SPT-N values of 0–1 blows/ft and medium-stiff clay with SPT-N values of 6–9 blows/ft in which the undrained shear strength of both clay layers are about 17–23 kPa and 34–47 kPa, respectively. The thicknesses of those layers are relatively thin (only approximately 2 m for each layer) comparing to the 3rd sand layer. The 4th clay layer

Fig. 1 Project location in Vietnam

is encountered between the depths of 35 m and 50 m. This clay layer is impermeable, very stiff. Its undrained shear strength is about 170–270 kPa. Since the toe of the D-wall was embedded in this layer, it plays a vital role in keeping the stability and limiting the movement of the D-wall. The 5th layer is a very dense sand layer. The sand is found at the depth of 50 m, with the SPT-N value in the range of 25–52 blows/ft. This layer has a negligible impact on the excavation since the final depth of the excavation did not reach this layer.

2.2 Instrumentations and Observed Behaviors of the Deep Excavation

Observation of retaining structures and adjacent buildings during excavations is vital for mitigating problems such as the instability and the excessive lateral movement of retaining walls, collapse and underground erosion of adjacent buildings, etc. For this purpose, seven inclinometers were installed inside the D-wall (ID01 to ID07), fourteen settlement points were installed on the ground surface (G1 to G14), twenty-one settlement points were installed on the adjacent building (B1 to B21), and six monitoring points (MW1 to MW6) were installed around the excavation area. The locations of these measurement points are shown in Fig. 4.

In this study, two-dimensional FEA was performed by commercial software, Plaxis 2D (2019). The inclinometers ID02 and ID06, located on the central sections of the longest side of the excavation, were chosen for calibrating FEA input parameters since they were less affected by the 3D corner. According to previous studies by Ou et al. (1996) and Hsiung et al. (2016), the 3D corner effect can be neglected if the plane strain ratio (PSR) is closely 1. The PSR is a ratio of the maximum wall deflection that can be used to transfer 2D FE results to 3D FE results. The PSR depends on the excavation
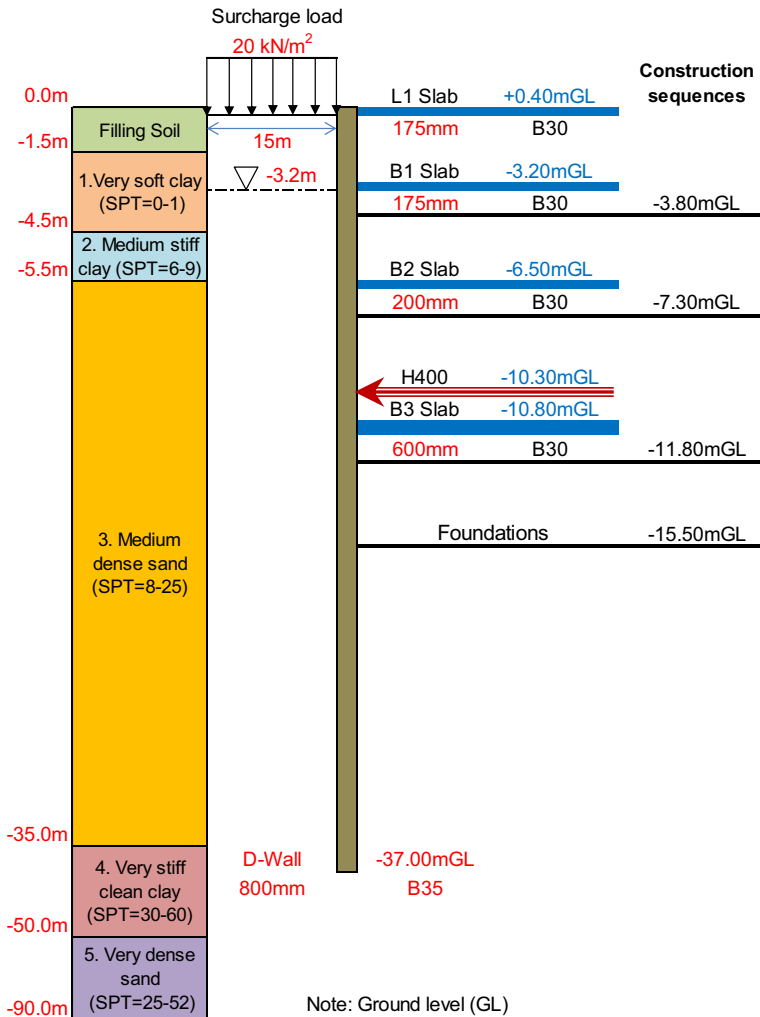
Fig. 2 Construction section and soil profile

aspect ratio B/L and the distance (*d*) from the evaluated section to the excavation corner. The PSR ratio was firstly proposed by Ou et al. (1996) for a typical excavation in clayey soils and then modified by Hsiung et al. (2016) for the one in sandy soils.

Table 1 Construction sequences of Madison project

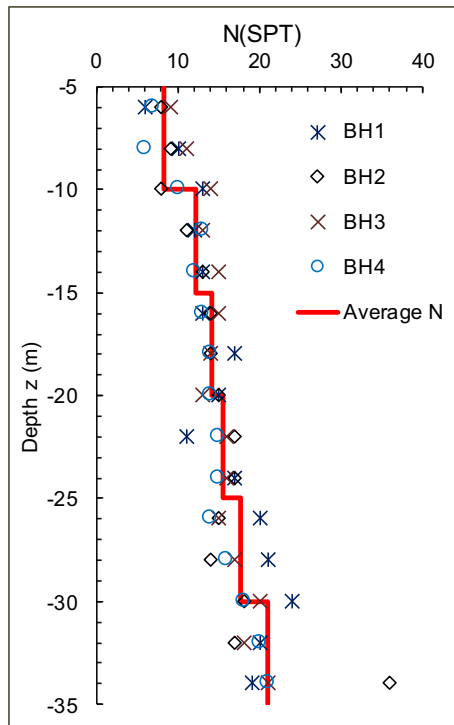| Stages	Construction sequences	Finishing date
1st	Excavation to − 3.8 mGL, and install B1 slab and L1 slab.	31/03/2017
2nd	Excavation to − 7.3 mGL, and install B2 slab.	26/04/2017
3rd	Excavation to − 11.8 mGL, install H400 steel struts at − 10.3 mGL	25/05/2017
4th	Excavation to the bottom level of foundations − 15.5 mGL	27/06/2017

Fig. 3 The variation of SPT-N values with the depth z in 3rd layer (the thick sand layer)

According to the chart proposed by Hsiung et al. (2016), the PSR value of the ID02 point can be considered 1 because the B/L value is about 0.56 (excavation width $B = 37$ m and excavation length $L = 65$) and the d value is about 32 m. Meanwhile, other inclinometer points had the PSR value in the range of 0.60–0.85. Note that the PSR
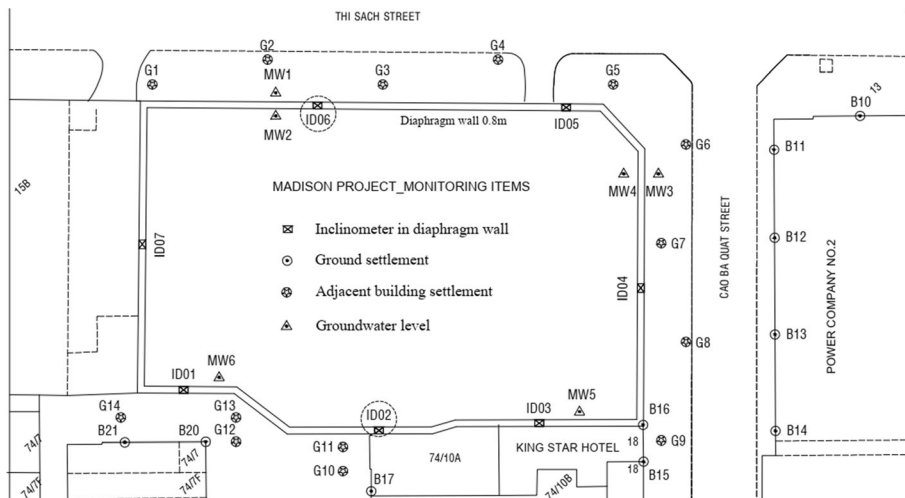

Fig. 4 The layout of monitoring points and adjacent buildings

ratio of the ID06 point is about 0.85. Lateral displacement profiles of the D-wall at ID06 and ID02 are shown in Fig. 5a and b. The figure indicates the similarity of the shape aspect of the lateral deflections with the difference in the magnitudes. It is also found that the maximum lateral displacements of ID06 point are approximately 10% lower than those of ID02 point. This is due to that the PSR ratios between both points are 0.85 and 1, which are very close to each other. Thus, it is assumed that the D-wall displacement at ID02 point is almost in the plane strain condition. The maximum horizontal displacement at the final excavation stage is approximately 32.9 mm at − 15.5 mGL. The percentage of the D-wall displacement is 0.4% of the excavation depth (H). These results are consistent with the range of 0.2–0.5% of the excavation depth by the study of Ou et al. (1993) for general excavation cases and the range of 0.15–0.6% of the excavation depth by the study of Hung and Phienwej (2016) for historical excavation cases using D-wall in Ho Chi Minh City.

Figure 6 shows the variation of groundwater inside and outside the excavation area during construction. In the pre-excavation stage, the average depth of initial groundwater was − 3.2 mGL below the ground surface. During construction, groundwater inside the excavation area was continuously kept to at least 1 m below the excavated level. Since the toe of the D-wall was embedded in an impermeable stiff clay layer, the level of monitoring groundwater outside the excavation was considerably unchanged until the end of the excavation. The condition of groundwater level inside and outside the excavation was considered in the FEA.

To measure the ground surface settlements, 14 monitoring points were installed at the outside perimeter of the excavation with a distance between 2 and 6 m from edges
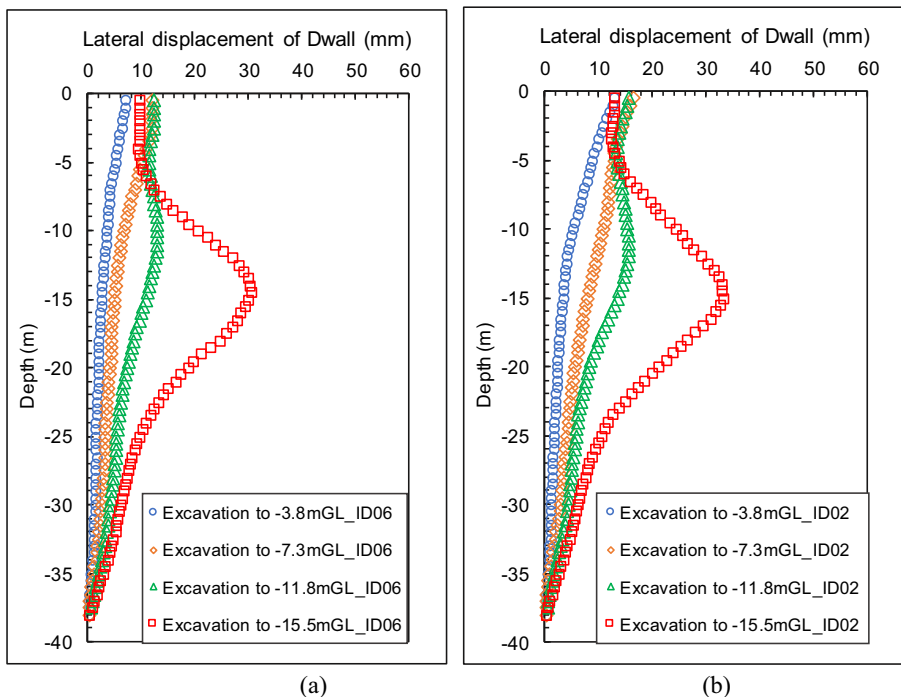

Fig. 5 Observed lateral displacement of D-wall at each excavation stages: **a** ID06 point; **b** ID02 point
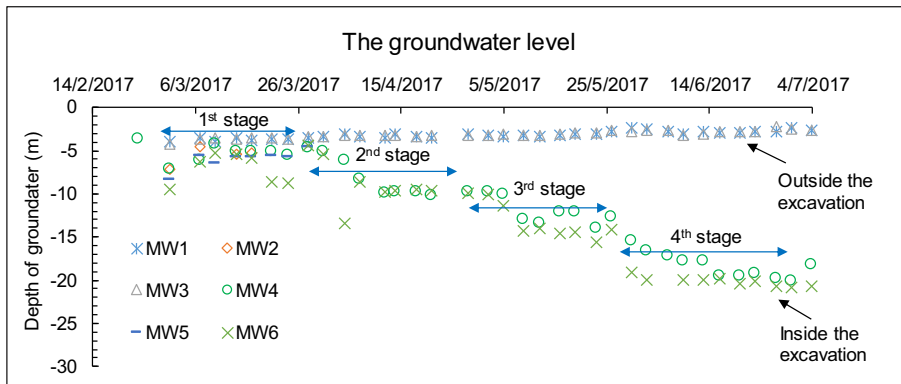
Fig. 6 Field observation of groundwater levels inside and outside the excavation during excavation stages

of the excavation. However, some monitoring points, such as G3 and G9, were failed during the monitoring campaign due to the heavy site traffic and incautious protection. Figure 7 presents recorded ground surface settlements during construction. The measurements indicate that the corners of the excavation zone, such as G1, G5, G6, G9, G13, and G14, settled less than other points by 20 to 50% (3 to 8 mm). The main reason is that the deformations of the ground surface were induced by the lateral displacement of the D-wall (Hsieh and Ou 1998; Ou and Hsien 2000), which were influenced by the 3D corner effect (Ou et al. 1996; Hsiung et al. 2016). The maximum ground surface settlement (δ_{vm}) reached approximately 14 mm at the G11 point, which is located at the center of the long side of the excavation zone. The minimum surface settlements belonged to points located near the corner of the excavation zone, which was only 0.34 mm, 1.70 mm, and 2.26 mm for G1, G6, and G14 points, respectively. The maximum ratio δ_v/H was about 0.09%, which was smaller than the proposed value by Clough (1990) in which the average value of the maximum surface settlement was about 0.15%H. The reason is that the monitoring points were not installed at the concave curve locations that have the maximum surface movement, which was at the location of 0.5H from the excavation edge according to the study by Hsieh and Ou (1998).
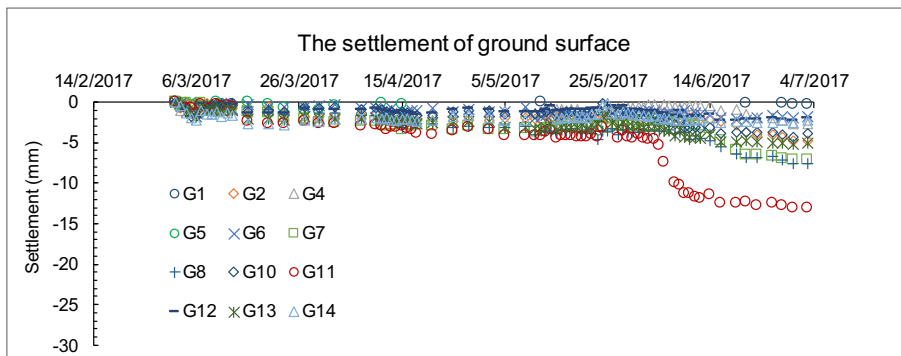

Fig. 7 Field measurement of ground surface settlement during the construction process

2.3 Adjacent Buildings

Low-rise and high-rise buildings adjacent to the excavation were surveyed during the pre-construction phase. The layout of adjacent buildings is shown in Fig. 4. The high-rise buildings, such as the King Start Hotel, Power Company No. 2, 15B, were supported by pile foundations. They were not significantly impacted by induced ground deformation during excavation. The low-rise buildings, such as the 74/10A, 74/10B, 72/7, and 74/7F buildings, are 1~3 story buildings supported by shallow foundations. The damage potential of the 74/10A building is the highest since the building is located on the center of the long side of the excavation zone. It can be seen from Fig. 8 that the settlements of buildings on piles were very small (less than 3 mm), for instance, at the observed points of B11 to B15. On the contrary, the maximum settlement at the 74/10A building located near ID02 point was approximately 20 mm. Several points at the corners of the excavation displayed the small settlement value of about 5 mm although the buildings with shallow foundations were located around those areas. Note that the damage on the 74/10A building was significantly influenced by the lateral deflection of the D-wall. The other adjacent buildings were not damaged or negligibly influenced by the lateral defection of the D-wall.

With the identification of the negative impact on adjacent buildings in the initial design stage, a careful investigation of the main structure and damage status of the 74/10A building was carried out in the pre-construction stage. In this stage, the building was in normal serviceability without any visible cracks on the external brickwork, masonry, or plaster ceiling. Figure 9 demonstrates the geometric dimension of the building plan in which there is a 3-story building with a height of 3.3 m per story. Investigated geometric dimensions of main building structures were 100 mm of floor thickness, 200×300 mm of beam width and height, 200×200 mm of column width and height, 12.0×1.2 m of shallow foundation width, and length, and the spacing of 4.0 m ($L_{spacing} = 4.0$ m). Unfortunately, visible cracks appeared on the external brickwork and plaster ceiling as well as at the corner of windows of the building when excavation was advanced to -15.5 mGL in the 4th excavation stage. The building was carefully re-surveyed and measured for evaluating the damage level. The investigation showed that there were 18 new visible cracks with the width varying from 0.2 to 0.7 mm and the length varying from 25 to 149 cm. The damage level of the 74/10A building is presented in Fig. 10. With full
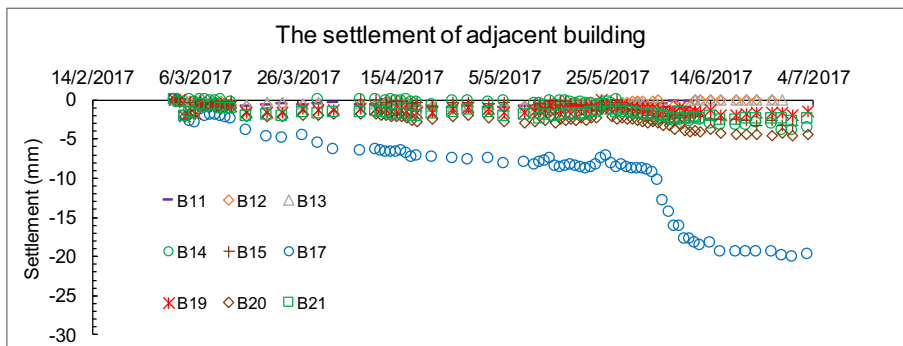

Fig. 8 Observation of adjacent building settlement during construction process
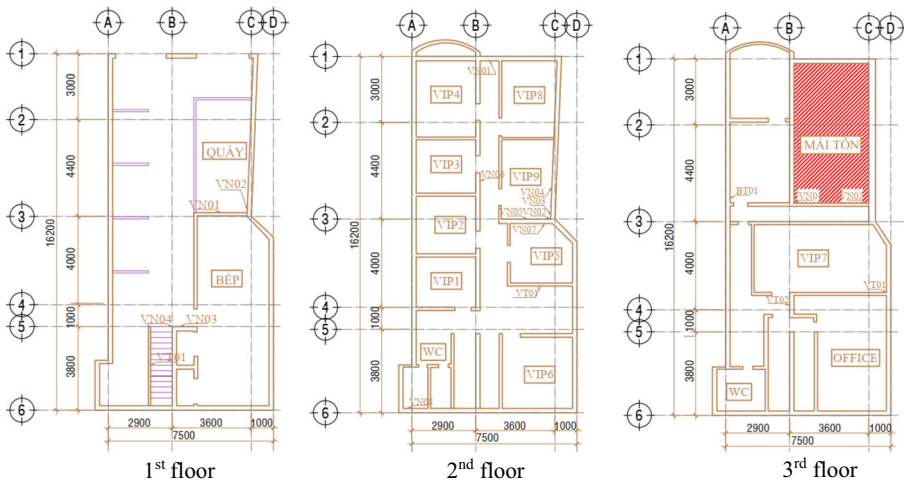
Fig. 9 The structural plan and geometric dimension of the adjacent building 74A/10

observation, the 74/10A building was chosen for analyzing and assessing the damage potential by FEA.

3 Numerical Model and Verification

3.1 Soil Parameters

In this study, soil stiffness parameters were calibrated with field measurements by the back-analysis technique using the hardening soil (HS) model. The soil parameter calibration by the back-analysis technique is not uncommon in the geotechnical field, for example, tunnel excavations (Sakurai and Takeuchi 1983; Gens et al. 1996; Sakurai et al. 2003), consolidation and testing embankments on soft clay (Arai et al. 1986), deep excavation (Finno and Calvello 2005; Zhang et al. 2015; Zhang et al. 2018a), and the stiffness parameters of different soils (Tan and Chow 2008; Teo and Wong 2012; Khoiri and Ou 2013; Likitlersuang et al. 2013; Hsiung and Dao 2014).

HS model is an advanced soil model based on the isotropic hardening (Schanz et al. 1999) with basic characteristics as follows: the stress-dependent stiffness according to the power law as expressed in Eq. 1, the plastic straining due to both primary deviatoric loading (shear hardening) and the primary compression (compression hardening and cap yield), the elastic un/reloading, the dilatancy effect, and the Mohr-Coulomb failure criterion. The HS model is commonly used in deep excavation analyses; it gives more realistic predictions of the lateral displacement of retaining wall and surface ground settlement than the Mohr-Coulomb or soft soil model (Teo and Wong 2012; Khoiri and Ou 2013; Likitlersuang et al. 2013). In the HS model, the soil stiffness is described much more accurately by the triaxial loading stiffness E_{50}, the triaxial unloading stiffness E_{ur}, and the oedometer loading stiffness E_{oed}. Almost parameters in the HS model are commonly defined from laboratory tests such as the consolidated-drained triaxial test (CD) and the oedometer test (OED). The E_{50} and E_{50}^{ref} represent the secant stiffnesses at
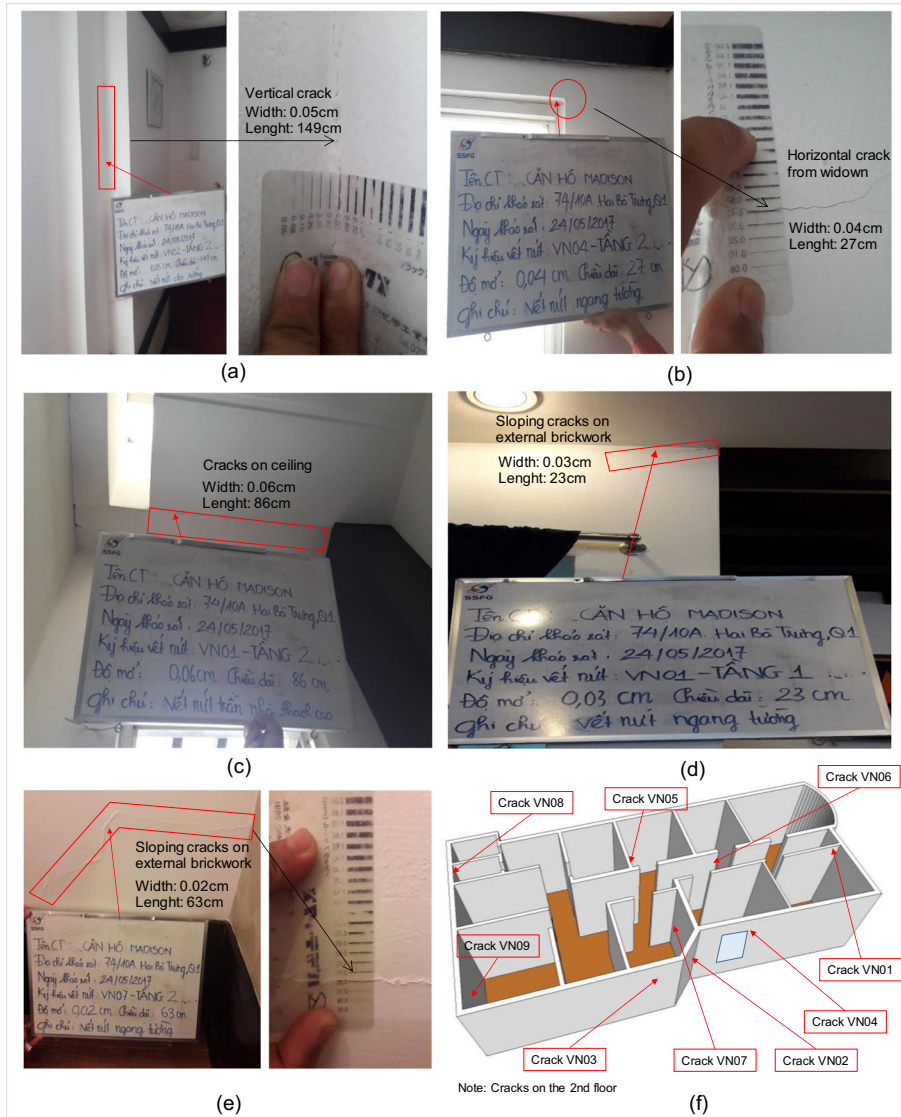
Fig. 10 Observed field cracking on the adjacent building 74A/10

pressure level σ'_3 and the reference pressure level P_{ref}, respectively. E_{50}^{ref} is commonly used as the input parameter while E_{50} is automatically calculated from Eq. 1.

$$E_{50} = E_{50}^{ref} \left(\frac{c' \cos\varphi' + \sigma'_3 \sin\varphi'}{c' \cos\varphi' + P_{ref} \sin\varphi} \right)^{m} \qquad (1)$$

In the above equation, σ'_3 denotes the minor effective principal stress, m is the law power, and P_{ref} denotes the preference pressure corresponding to E_{50}^{ref} (Plaxis 2019).

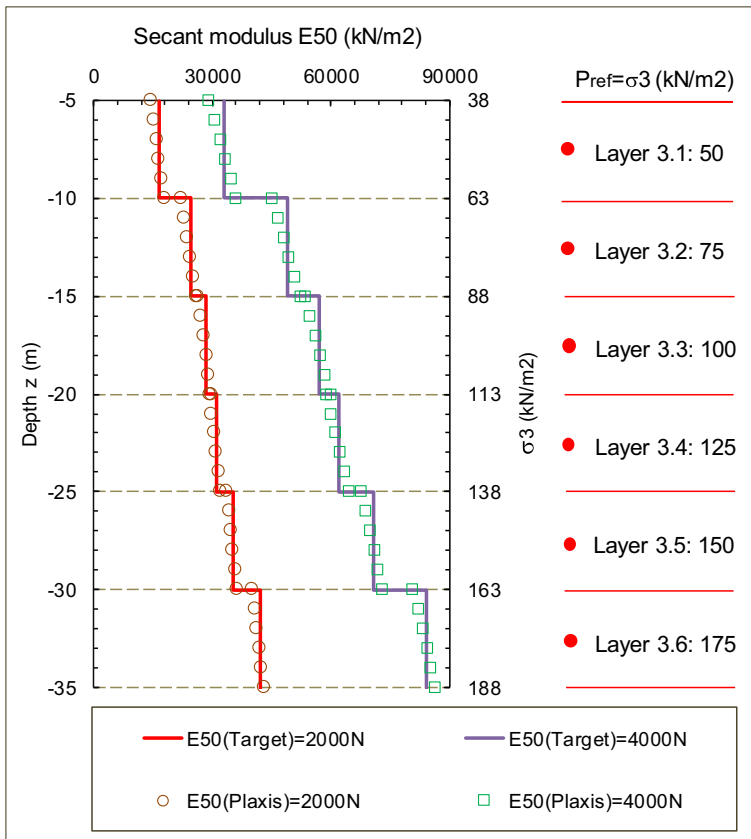**Fig. 11** The secant stiffness E_{50} according to SPT-N value and the reference pressure P_{ref} at depths (z)

The clay layers were adopted in total stress undrained analysis with a friction angle $\varphi_u = 0$ and undrained shear strength $c_u = S_u$. In that case, the E_{50} is equal to the E_{50}^{ref} according to Eq. 1. The secant modulus for clay soils can be determined by empirical equations (Lim et al. 2010; Hsiung et al. 2016; Yong and Oh 2016). The E_{50}^{ref} equals to $300S_u$ in the case of soft soil and $500S_u$ for stiff clay.

Table 2 Input parameters for soil layers

Soil layer	Depth (m)	SPT-N (value)	φ' (deg)	c' (kPa)	S_u (kPa)	E_{50}^{ref} (kPa)	E_{oed}^{ref} (kPa)	E_{ur}^{ref} (kPa)	m
1. Very soft clay	1.5–4.5	0–1	–	–	17–23	$300S_u$	E_{50}^{ref}	$3E_{50}^{ref}$	1
2. Medium stiff clay	4.5–5.5	6–9	–	–	34–47	$500S_u$			0.8
3. 1–3.6 Medium dense sand	5.5–35	8–25	26–28	5–8	–	2000 N–4000 N			0.5
4. Very stiff clay	35–50	30–60	–	–	170–270	$500S_u$			0.7
5. Very dense sand	50–90	25–52	31–33	5–10	–	2000 N			0.5

In terms of sandy soils, good-quality samples are comparatively difficult to obtain. The strength parameter of sandy soil named φ′ (effective stress friction angle) can be directly determined from the laboratory tests such as the direct shear test, and trial shear test. The φ′ value is dependent on the surface roughness and the shape of sand particles and is independent of the stress state (Alshibli and Alsaleh 2004; Altun et al. 2011; Sadrekarimi and Olson 2011). However, the stiffness parameter E' is significantly influenced by physical properties, field sample density, and interactive force of the sand grains, which are mainly impacted by the sample disturbance. The stiffness parameters are commonly estimated from the SPT-N value in practice. Some empirical correlations of SPT-N value with soil stiffness and shear strength were proposed by Stroud (1989) from the collected data of different soil types. The correlation between E and N for sand soil is in the range of 2000N and 4000N (e.g., Stroud 1989; Tan and Chow 2008; Hsiung 2009; Shukor 2009; Hsiung et al. 2016; Yong and Oh 2016). Hsiung (2009) and Hsiung et al. (2016) proposed E_{50} to be 2000N by conducting a series of back-analyses of monitoring data in Taiwan. The E value of 2000N was suggested for deep basement designs in Malaysia by Tan and Chow (2008). Stroud (1989) suggested that E decreases as the soil strain increases. The E can be equal to 4000N within the strain range of a retaining wall (0.1%) (Yong and Oh 2016). AIJ (2001) recommends the E value of 2800 N in common geotechnical practice. The E value of 3500 N was proposed by Shukor (2009) based on a back-analysis of lateral displacement of the cantilever diaphragm wall. From the above review results, the E values in the range of 2000–4000N were selected for back-analysis in this study. It is noted that SPT values had considered to measure shear strength reflected by shear wave velocity in some cases (Mase 2017; Misliniyati et al. 2019; Likitlersuang et al. 2020).

Note that it is not easy to set up the preferred value of E_{50} in the HS model because of the considerable increases of the SPT-N value with depth z. The variation of E_{50} according to N(SPT) values for a thick sand layer over 30 m cannot be reproduced in a single sand layer by Eq. 1. To avoid this difficulty, the thick sand layer (3rd layer) was divided into several sub-layers. The p^{ref} value of each sub-layer is assumed to be the σ′$_3$ at the middle of the layer, and the E_{50}^{ref} is calculated from the average SPT-N value of the layer. Figure 11 demonstrates comparisons of targeted E_{50} and the actual calculated E_{50} in the HS model. In this figure, the solid lines and unfilled markers represent the targeted E_{50}, E_{50}(Target), and actual calculated E_{50}, E_{50}(Plaxis), respectively. For the other stiffness parameters, the E_{ur} and E_{oed} values are assumed to be $3E_{50}$ and E_{50}, respectively (Schanz et al. 1999; Schweiger 2009; Teo and Wong 2012). All soil parameters were summarized in Table 2.

3.2 Structural Parameters

The D-wall was simulated by plate elements equipped with zero-thickness interface elements (Khoiri and Ou 2013; Plaxis 2019). The reduction factor of the interface element ranges between 0.5 ~ 1.0 depending on soil and retaining wall materials as well as the degree of soil disturbance during constructions. The basement slabs and the steel struts were simulated by fixed-end anchor elements. The linear elastic model was adopted for the D-wall, basement slabs, and steel struts (Ou et al. 1996; Lin et al. 2016; Zhang et al. 2019; Huynh et al. 2020a; Zhang et al. 2020). The axial stiffness (EA) of the basement slabs shown in Table 3 was determined by a structural software

Table 3 Input parameters of structures for Plaxis 2D model

Parameters	EA (kN/m)	EI (kNm²/m)	w (kN/m/m)	ν	$L_{spacing}$ (m)	L (m)
D-wall	24×10^6	1.28×10^6	6.4	0.15	–	–
L1 slab	27×10^3	–	–	–	1.0	1.0
B1 slab	70×10^3	–	–	–	1.0	1.0
B2 slab	150×10^3	–	–	–	1.0	1.0
H400	165×10^3	–	–	–	7.5	–

L is the length of fixed-end anchor in Plaxis 2D model

considering the percentage of openings in the slabs. The axial stiffness (EA) is based on the elastic relationship between unit force P(kN) and corresponding displacement Δy(m) as Eq. 2. In which L is the length of fixed-end anchor in the model Plaxis,

$$EA = \frac{PL}{\Delta y} \tag{2}$$

In the 2D FEA, the adjacent building was simulated as a flat framed structure including floors, beams, columns, and foundations. This adoption has been successfully applied in several previous studies (Cording et al. 2010; Sabzi and Fakher 2015; Zhang et al. 2018b; Huynh et al. 2020b). The structures in this study were modeled by plate elements with flexural stiffness EI (kN/m²/m) and axial stiffness EA (kN/m). The actual dimensions of the 74/10A building structures were mentioned earlier in Section 2.3. The 2D framed stiffness was computed per 1 m unit in the plane strain model. The total stiffness of the floor and the beams was divided by corresponding spacings as expressed by Eq. 3. Dead and live loads of the building were directly added to the weight of the plate element (w). Table 4 presents the input parameters of the structural element for FE modeling.

$$EI_{1m} = \frac{EI_{floor} + EI_{beams}}{L_{spacing}} \tag{3}$$

$$EA_{1m} = \frac{EA_{floor} + EA_{beams}}{L_{spacing}} \tag{4}$$

3.3 Boundary Conditions and Groundwater Calculations

Figure 12 illustrates the cross-section of deep excavation adopted for the simulation as well as the mesh generation of FEA. The length of the cross-section of the domain is

Table 4 Input parameters for 2D frame structure

Parameters	EA (kN/m)	EI (kNm²/m)	w (kN/m/m)	ν
Floor + beam	3,105,000	5287	6.00	0.15
Column	270,000	900	0.25	0.15
Foundation	6,500,000	350,000	5.60	0.15

37 m obeying the actual design of the basement. The bottom of the FEA mesh was set at 80-m depth which is located in the very dense sand layer. The lateral boundary was set at about 80 m from the D-wall, which is more than four times of the final excavation depth ($d > 4H$) and over two times of the D-wall length ($d > 2$ L). It exceeds the zone of influence of the excavation deformation as suggested by Plaxis (2019) and the range of ground concave surface settlement (Clough 1990; Hsieh and Ou 1998). The horizontal movements are restrained at left and right boundaries while the fixed condition was applied to the bottom of the FEA mesh.

For the hydraulic boundary condition of the FEA, water was allowed to permeate through lateral boundaries while the impermeable condition was assumed at the bottom boundary. To simulate dewatering inside the deep excavation, the initial groundwater level was set at 3.2 m below the ground surface based on data from monitoring wells, and the steady-state groundwater flow calculation was simulated as suggested by Plaxis (2019). The seepage from the outside to the inside of the deep excavation and the active pore-water pressure on the D-wall were maintained during excavation. Figure 13 demonstrates the comparisons of the groundwater level outside and inside the excavation from FEA and field observation. The outside groundwater level is almost stable during the excavation sequence, which agrees with the field observations. However, in the final stage, monitoring groundwater level outside the excavation increased very slightly, because it might be influenced by uncertain factors such as rain, flow, and river water level. The observed water table in the excavation area was lower than the excavation level between 1 and 3 m and well consistent with the FEA results.

3.4 Verification of FE Analysis

To obtain a good agreement between the predicted and observed D-wall displacement, the authors performed a parametric study by varying the stiffness E_{50} in the range between 2000 and 4000N. Figure 14 illustrates the comparison between observations and simulations of lateral wall displacements at the final excavation stage. When the E_{50} is equal to 2000N, the predicted lateral displacements at the toe of the D-wall and the middle part significantly overestimate the observed values. Only the top of the D-wall more or less fits with the observed value. The maximum difference between the measured and calculated displacement is about 30% indicating the underestimation of soil-related stiffness. When E_{50} is adjusted to 4000N, the difference between the calculated lateral movements of the D-wall toe and the observed value is almost zero.
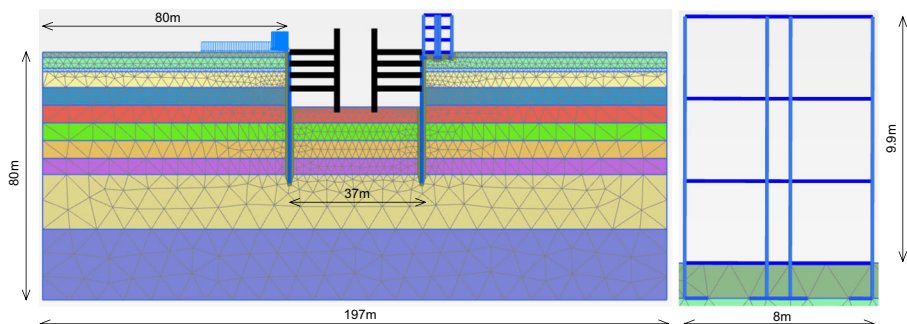

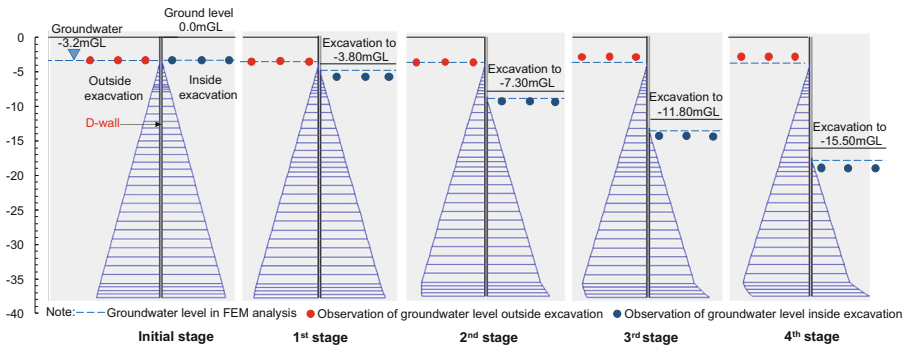**Fig. 12** 2-dimensional FE simulation by Plaxis 2D 2019

Fig. 13 Hydraulic condition in FE analysis and field observation

The predicted movements are 4.4 mm and 2.9 mm less than the observed values at the middle and the top of the D-wall, respectively. The predicted movements are about 15% lower than the measured one indicating the overestimation of soil-related stiffness. Based on these analysis cases, the secant modulus of the thick sand layer should be varying with depth and in the range of 2000–4000N. The suitable value of E_{50} was further explored by multiplying a constant value of 2000N by a modifier function, $F(z)$, which varies with depth (z) as Eq. 4. Note that the depth z should be in the range between 5 and 40 m.
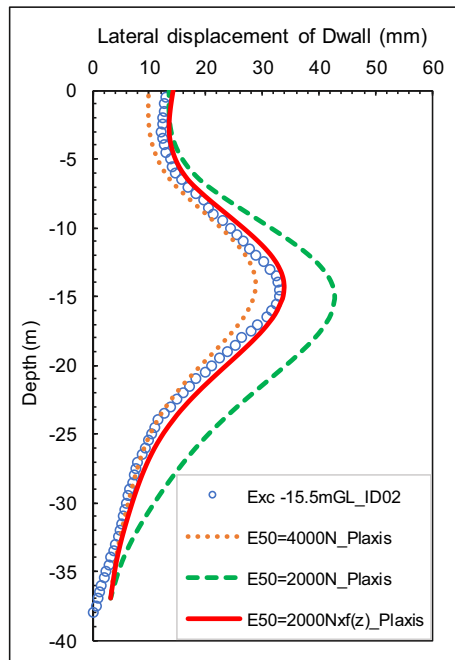
$$F(z) = 1 + (0.0286z - 0.1429)^{0.5}. \tag{5}$$

Fig. 14 Comparison of the predicted and observed horizontal D-wall displacement of various secant modulus at the final stage
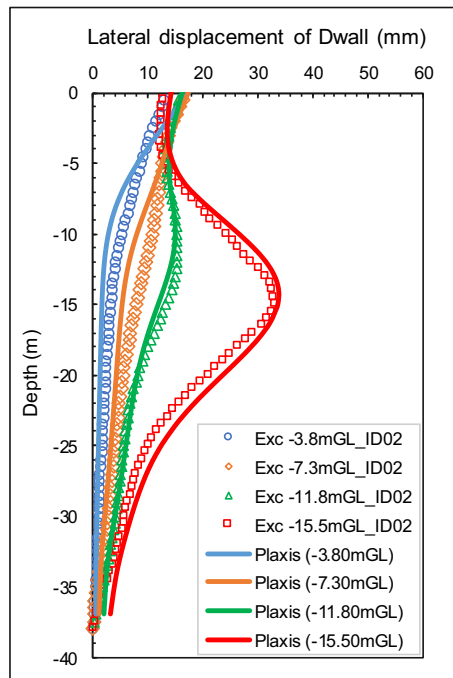
Fig. 15 Comparison of the predicted and observed horizontal D-wall displacement at all excavation stages

As seen from Fig. 14, a good agreement between field measurements and FEA can be obtained when the E_{50} was estimated by the proposed function. The predicted lateral displacements were 14.0 mm, 33.9 mm, and 7.2 mm at the top, the middle, and the toe of the D-wall, respectively (the corresponding observed values are 12.9 mm, 32.9 mm, and 6 mm, respectively). Comparing to the observed maximum lateral displacement in the middle part of the wall (32.9 mm), the total displacement errors at all wall parts between prediction and observation were about 5%. To confirm the validity of calibrated FEA, the predicted lateral displacements of the D-wall and the settlement of the adjacent building were compared with field measurements when the excavation depth was 3.8, 7.3, 11.8, and 15.5 mGL. As seen from Fig. 15 and Fig. 16, the prediction
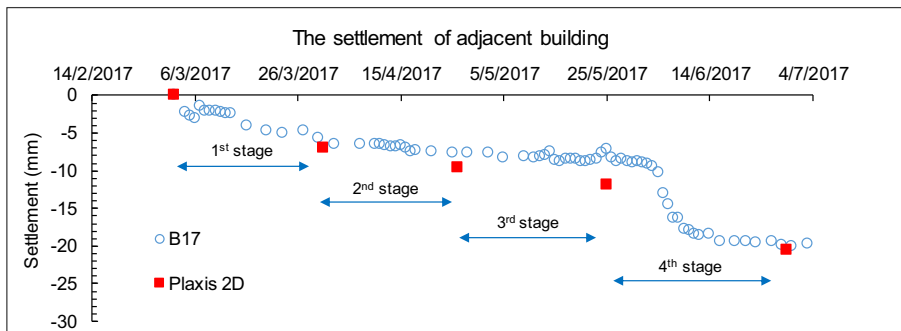

Fig. 16 Comparison of the predicted and observed adjacent building settlements at various excavation stages
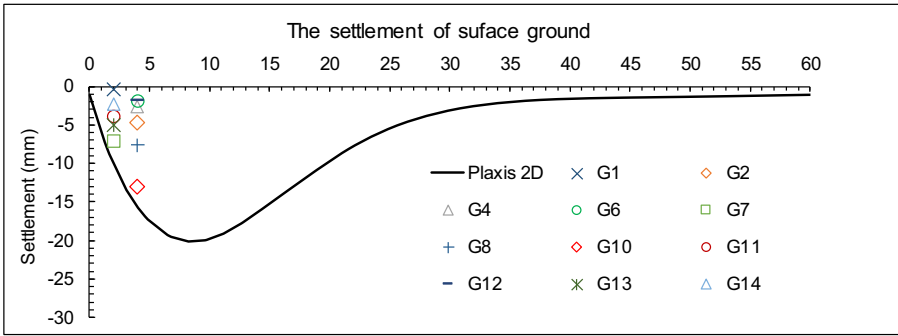
Fig. 17 Comparison of the predicted and observed surface ground settlement at the 4th excavation stage

using $E_{50} = 2000N \times f(z)$ agrees well with the measured displacements for all excavation stages.

Figure 17 compares the calculated and measured ground settlement in the final stage. The settlement at G10, which is the nearest to the ID02 inclinometer, was closer to the FE result than other points. It should be noted that the observed settlement at other points was smaller than that at the G10 point and the predictions under plane strain condition because of the influence of the 3D corner effect. The FEA indicates that 20.1 mm of the maximum ground surface settlement occurs at 8 m (0.5H) away from the excavation edge. The obtained results agree with the findings by Hsieh and Ou (1998). The ratio of the maximum ground surface settlement to the maximum wall displacements according to the FEA ($\delta_{vmax}/\delta_{hmax}$) is about 0.6. The FEA results are also close to this value in which $\delta_{vmax}/\delta_{hmax}$ is in the range of 0.5–0.75 as discussed in the works by Mana and Clough (1981) and Ou et al. (1993).

The tilt of the adjacent building at each construction stage is presented in Fig. 18. The building tilted toward the excavation in the 1st and 2nd stages and was larger than that that occurred in other states. The change in the tilt is due to the different curve shapes of ground deformations in each stage. The changes in the tilt also depend on the lengths and the locations of the buildings in the influence zone of the ground surface settlement.
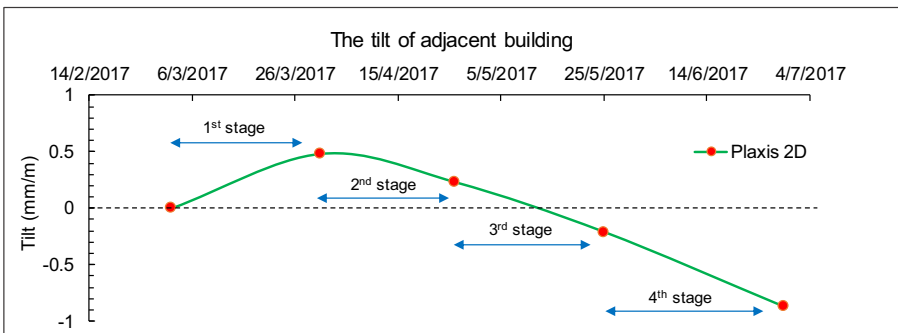

Fig. 18 The change in the tilt of the adjacent building according to excavation sequences. Note: θ = direction of crack formation and the angle of the plane on which ε_p acts, measured from vertical plane

4 Review of Evaluation Criteria of Building Damage Potential

Several criteria were proposed for assessing damage potential and damage levels of adjacent buildings caused by deep excavation. The main parameters for evaluation consist of the angular distortion β, the lateral extension strain ε_L, and the principal strain ε_p. Among these parameters, β is calculated from the average settlement slope minus the building tilt as presented in Eq. 5. This parameter, β, is relevant to diagonal cracks in affected buildings. The lateral extension strain ε_L is the deformation due to the lateral ground displacement, which is calculated by the lateral extension of a building base divided by its length as described in Eq. 6. This parameter, ε_L, is relevant to vertical cracks in affected buildings. The principal strain ε_p is assumed as the maximum strain on a building formed from the β and ε_L as shown in Eq. 7. Figure 19 demonstrates the details of this determination. Typically, the maximum principal strain ε_p is compared with the critical strain values of building damage classification to estimate damage levels. In some special cases, adjacent buildings with short lengths are mainly damaged by the angular distortion, where the influence of lateral strain is negligible.

$$\beta = \frac{\delta_v}{L} = \text{Slope(S)-Tilt(T)} \tag{6}$$

$$\varepsilon_L = \frac{\delta_L}{L} \tag{7}$$

$$\varepsilon_p = \varepsilon_L \cos\theta_{max}^2 + \beta \sin\theta_{max}\cos\theta_{max} \tag{8}$$
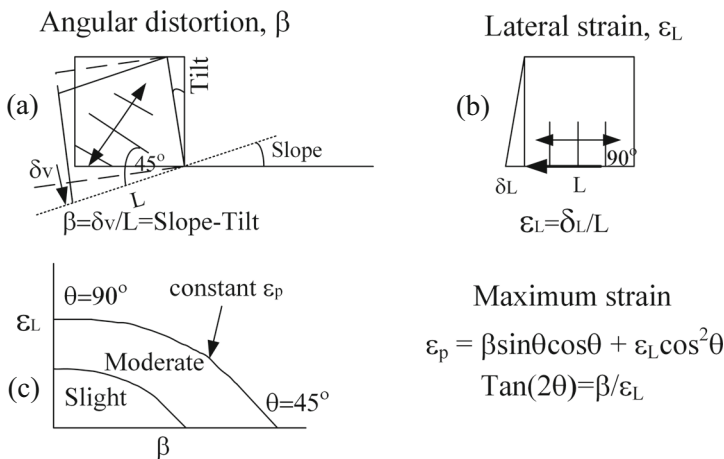
Note: θ = direction of crack formation and the angle of the plane on which ε_p acts, measured from vertical plane.

Fig. 19 Define angular distortion β, lateral strain ε_L, and maximum principal strain ε_P

In which $\mathrm{Tan}(2\theta_{\max}) = \frac{\beta}{\varepsilon_L}$.

In the above equations, L denotes the building length, δ_v denotes the forced distortion, δ_L denotes the forced lateral extension, β denotes the angular distortion, ε_L denotes the lateral strain, and $\theta_{\max}$ denotes the direction of crack formation measured from the vertical plane.

Burland (1977), firstly, proposed the damage levels for adjacent buildings by collecting and analyzing the data of the building damages observed from construction sites. Table 5 defines six levels of building damages, numbered from 0 to 5 with increasing severity, based on the criteria of severity degree such as the width of cracks or the limiting tensile strain of buildings. For instance, with a measured width of cracks less than 5 mm or calculated result of ε_p in the range of 0.75–0.15%, the damage level of the adjacent building is classified as level 2. Besides, a simple chart of strain state to evaluate building damage potential was also proposed as described in Fig. 19(c).

Boscardin and Cording (1989) extended the work of Burland (1977) and combined the previous building damage studies of Skempton and MacDonald (1956) and Bjerrum (1963). An updated practical chart of strain state for the estimation of building damage potential was proposed by Boscardin and Cording (1989) as indicated in Fig. 20. In Fig. 20, three categories of damage were classified by visible damage repairs, and six degrees of severity were classified by crack width. Three categories of damage are explained as follows;

- *Aesthetic damages* are related to slight cracks of building structures, affection mainly is easy to repair generally, and redecoration is sufficient to cover the light cracks.
- *Functional damages* are related to the loss of functionality or serviceability of parts of the building (e.g., doors and windows may be stuck and pipelines can be damaged) or of sensitive devices located inside the building (such as precision instruments that are sensitive to differential movements); the structural integrity of the building is not affected; however, the lack of serviceability can have commercial and economic impacts on the building and the host's activities.
- *Structural damages* are related to excessive cracks or deformations of bearing structures and can lead to the partial or total collapse of the building. Structural damages can sometimes remain partially hidden beneath the finishes. However, whitewash and plaster are good indicators of the cracking propagation.

In the recent study by Schuster et al. (2009), a new notion, called the damage potential index (DPI), was introduced for the evaluation of the damage potential of adjacent buildings. The DPI is a modification of the maximum principal tensile strain ε_p, which can be calculated from Eq. 8.

$$\mathrm{DPI} = \varepsilon_p/(1/200) \times 100 \tag{9}$$

Schuster et al. (2009) illustrated six damage levels of buildings associated with DPI values as presented in Table 6. In addition, to verify the damage classification according to DPI value, 75 historical excavation cases from the database of previous studies

Table 5 Damage classification established by Burland et al. (1977) and the relationship between the degree of damage and limiting tensile strain (after Boscardin and Cording 1989)

| Category of damage	Degree of severity	Description of typical damage	Crack width [mm]	Limiting tensile strain (%)
0 aesthetic	Negligible	Hairline cracks	<0.1	0–0.05
1 aesthetic	Very slight	Fine cracks which are easily treated using normal decoration. Damage generally restricted to internal wall finishes. Close inspection may reveal some cracks in external brickwork or masonry.	<1.0	0.05–0.075
2 aesthetic	Slight	Cracks easily filled. Redecoration probably required. Recurrent cracks can be masked by suitable linings. Cracks can be visible externally and some repointing may be required to ensure weather-tightness. Doors and windows may stick slightly.	<5.0	0.075–0.15
3 aesthetic/functional	Moderate	The cracks require some opening up and can be patched by a mason. Repointing of external brickwork and possibly a small amount of brickwork to be replaced. Doors and windows sticking. Service pipes may fracture. Weather - tightness often impaired. functional/serviceability	5–15 (many cracks with width > 3 mm)	0.15–0.3
4	Severe	Extensive repair work involving breaking-out and replacing sections of walls, especially over doors and windows. Windows and door frames distorted, floor sloping noticeably. Walls leaning or bulging noticeably, some loss of bearing in beams. Service pipes disrupted.	15–25 (but depend on the number of cracks)	>0.3
5 structural	Very severe	Structural damage which requires a major repair job involving partial or complete rebuilding. Beams lose bearing, walls lean badly and require shoring. Windows were broken with distortion. Danger of instability	>25 (but depend on the number of cracks)	
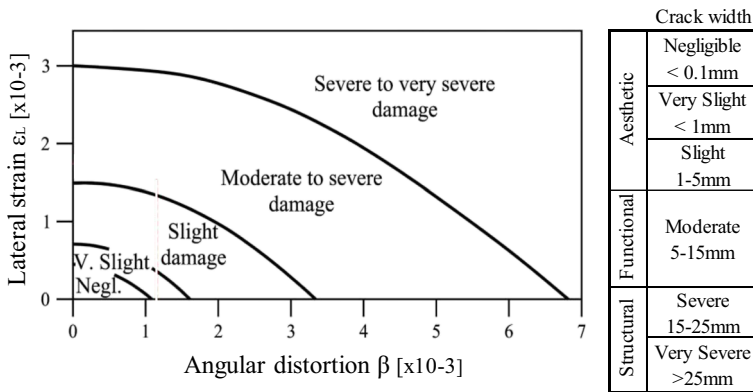
Fig. 20 Damage criterion based on the strain state of a point (after Boscardin and Cording 1989)

were evaluated in their study. The results indicated that the majority of the evaluated cases (approximately 80%) were correctly classified.

Comparing to previously proposed criteria, the advantage of the DPI concept is that it provides a relative measure of the maximum principal strain and a convenient approach of the damage potential evaluation. The damage levels of the building can be easily assessed in terms of relative DPI value. In this study, approaches proposed by Boscardin and Cording (1989) and Schuster et al. (2009) were employed to evaluate the damage potential of adjacent buildings.

5 Assessment of Damage Level on the Adjacent Building

To assess the damage levels of the adjacent building named 74/10A from the FE results, the simple chart of strain state proposed by Boscardin and Cording (1989) and the DPI value proposed by Schuster et al. (2009) were used in this part.

According to the field investigation, there are 18 new visible cracks with a width between 0.02 and 0.07 cm and the length from 25 to 149 cm as recorded in Fig. 10. These cracks were easily treated by normal decoration to cover the visible cracks. According to Burland (1977), visible cracks with the width being smaller than 5 mm are categorized as aesthetic damages with the degrees of severity from very slight to slight conditions.

Table 6 Levels of building damage according to DPI

Level of building damage caused by excavation		DPI (damage potential index)
0	Negligible to very slight	0–15
1	Very slight to slight	15–25
2	Slight to moderate	25–35
3	Moderate	35–60
4	Severe	60–85
5	Very severe	> 85

In the 1st and 2nd stage, no cracks or damages were observed. Little fine cracks in the internal brickwork of the building were noticed when the excavation depth was 11.8 mGL. In the 4th stages of the excavation which the excavation depth was 15.50 mGL, visible cracks were readily observed in the internal and external brickwork, masonries, and plaster ceilings. Some cracks were at window corners. However, the adjacent building is still in a good serviceability condition. No visible crack was observed on main structural elements such as slabs, beams, and columns.

Based on the calculated displacements of structural elements of the adjacent building and the ground surface from the FEA, the angular distortion β and lateral strain ε_L of the adjacent building are determined according to Eq. 5 and Eq. 6, respectively. The movements of the ground surface and the adjacent building structures at the 4th excavation stage are shown in Fig. 21. This figure illustrates a cross-section of the adjacent building including height building (H), isolated bay length (L), distance to the
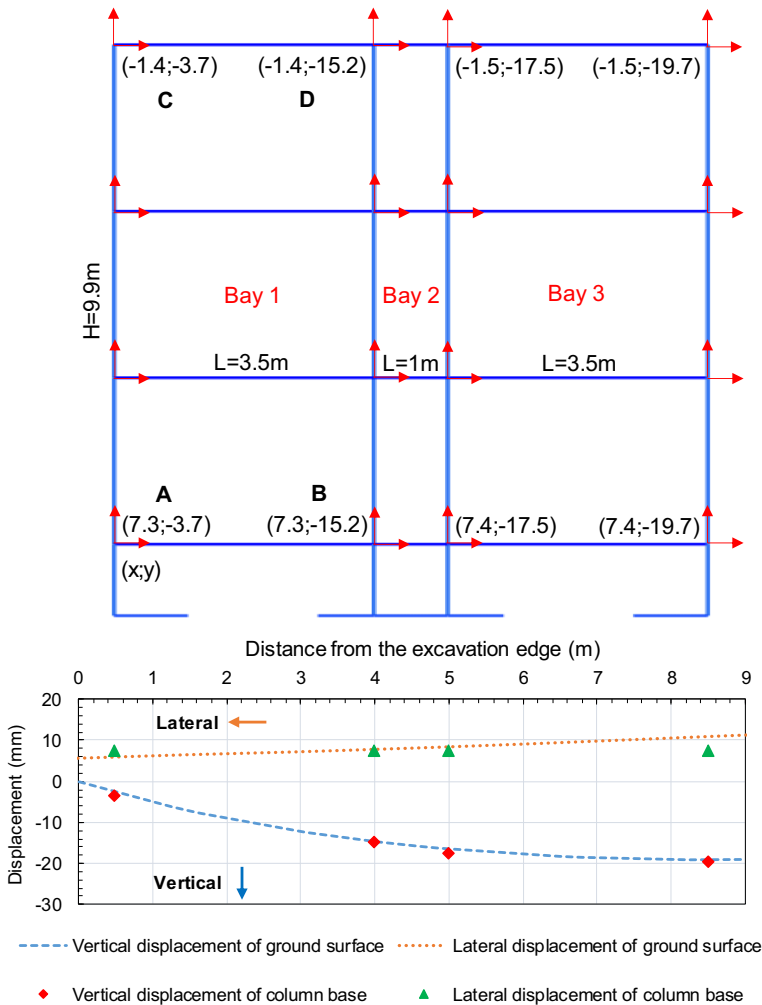
Fig. 21 Movement of the ground surface and adjacent building structures in the 4th excavation stage

excavation edge, and nodal points of the frame structure. In that, the x, y values (x,y) are the vertical and horizontal displacements of the nodal points obtained from the FEA. Besides, the lateral and vertical displacements of the ground surface and isolated column bases are described by dotted lines and filled markers, respectively, in the chart. The slope of Bay no. 1 is determined from the vertical movements of nodal points A, B, C, and D as expressed by Eq. 9. Equation 10 demonstrates the determination of the tilt of a bay from the horizontal displacements of nodal points and the building height. The lateral extension, ε_L, was calculated from the difference between lateral movements at two ends of a beam element by Eq. 11. The calculations for other bays are similar to that of Bay no. 1. Table 7 summarized the calculated results of all bays from all excavation stages.

$$\text{Slope}(S) = \frac{(y_A\text{-}y_B) + (y_C\text{-}y_D)}{L_{AB} + L_{CD}} \tag{10}$$

Table 7 Calculation of ground slope, building tilt, lateral strain ε_L, angular distortion β, and damage potential index (DPI) at excavation stages

Span	Bay 1	Bay 2	Bay 3
1st excavation to − 3.8 mGL			
Ground slope	0.57	0.89	1.05
Tilt	0.48	0.48	0.48
Angular distortion β	0.09	0.41	0.57
Lateral strain ε_L	0.00	0.00	0.00
DPI value	1.00	4.10	*5.70*
2nd excavation to − 7.3 mGL			
Ground slope	− 0.31	− 0.43	− 0.61
Tilt	0.23	0.23	0.23
Angular distortion β	0.54	0.66	0.84
Lateral strain ε_L	0.00	0.00	0.00
DPI value	5.40	6.60	*8.40*
3rd excavation to − 11.8 mGL			
Ground slope	− 1.33	− 0.67	− 0.57
Tilt	− 0.21	− 0.21	− 0.21
Angular distortion β	1.12	0.46	0.35
Lateral strain ε_L	0.00	0.00	0.00
DPI value	*11.20*	4.50	3.50
4th excavation to − 15.50 mGL			
Ground slope	− 3.28	− 2.30	− 0.63
Tilt	− 0.87	− 0.87	− 0.87
Angular distortion β	2.41	1.43	0.24
Lateral strain ε_L	0.00	0.00	0.00
DPI value	*24.10*	14.3	2.40

$\times 10^{-3}$

$$\text{Tilt(T)} = \frac{(x_c - x_A) + (x_D - x_B)}{H_{AC} + H_{BD}} \tag{11}$$

$$\varepsilon_L = \frac{\delta_L}{L} = \frac{(x_A - x_B) + (x_C - x_D)}{L_{AB} + L_{CD}} \tag{12}$$

The calculated values of β and ε_L and the damage criteria proposed by Boscardin and Cording (1989) are shown in Fig. 22. The calculated results almost indicate negligible to slight damage potentials. Additionally, the DPI values are also determined by Eq. 4 and shown in Table 7. The maximum DPI values at each excavation stage varied from 5.7 to 24.1. It means that the damage potential varies from very slight to slight conditions. Table 8 demonstrates the comparison of estimated damages by two criteria using field observations and FEA predictions. The evaluated damages are completely consistent with the observed ones in the field as the comparisons are shown in Table 8.

In the first stage, the highest DPI value of 5.7 occurs at the farthest bay from the excavation. However, the highest DPI of 24.1 was observed at the nearest bay in the final stage. The compelling reason is that the influence zone and the ground concave surface of the settlement expands as the excavation depth increases. According to Clough (1990) and Ou and Hsien (2000), the influence zone is the distance of two to three times of the excavation depth (H) from the excavation edge. The maximum ground surface settlement occurs approximately within half of the excavation depth from the edge of the D-wall (Hsieh and Ou 1998).

For more discussion, Table 7 also shows the values of lateral strain ε_L of the adjacent building in all excavation stages. The ε_L values are approximately equal to zero because the absolute lateral movement of isolated columns is similar, for example, in the final stage, this movement is approximately 7.3 mm as shown in Fig. 21. It means that the tensile strains in the beams and the floors were not developed in the adjacent building in this case.
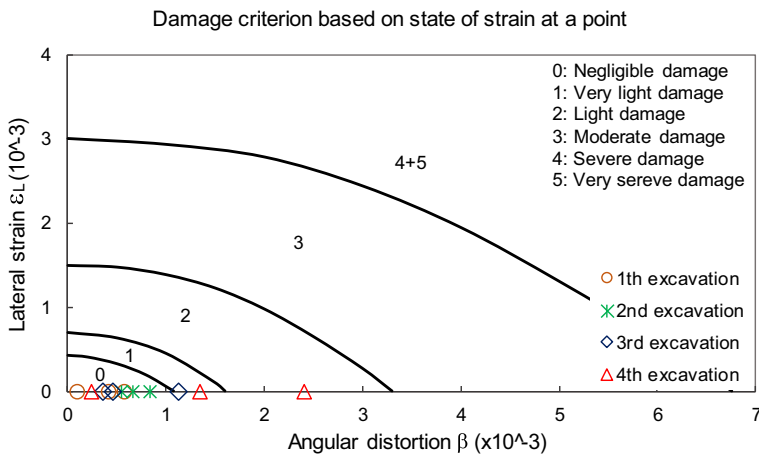

Fig. 22 Assessing the adjacent building damage potential according to the simple chart of Boscardin and Cording (1989)

Table 8 Comparisons of damage levels of adjacent building based on FE analysis and field observation

Construction sequences	FE analysis			Field observations of damage
	Damage assessed by Boscardin and Cording (1989).	Damage assessed by Schuster et al. (2009)		
		DPI max	Damage level	
1st excavation to − 3.8mGL	Negligible	5.7	Negligible	No damage
2nd excavation to − 7.3mGL	Negligible	8.4	Negligible to very slight	No damage
3rd excavation to − 11.8mGL	Very slight	11.2	Negligible to very slight	The first cracks appeared in external brickwork, masonry and ceiling
4th excavation to − 15.50mGL	Slight	24.1	Very slight to slight	The cracks have widened in brickwork, masonry and ceiling with the width of 0.2–0.7 mm and length of 25-149 cm

6 Conclusions

This paper investigates the behavior of deep excavation and adjacent building including the lateral movements of the D-wall, the ground surface settlements, the adjacent building tilts, and the damage of adjacent buildings based on an excavation case in a sand thick layer in Vietnam. The findings from the study can be summarized as follows:

1. The percentages of the lateral displacements of the D-wall are 0.4% and 0.2% of excavation depth (H) for the cantilever and braced excavations, respectively. The FEA indicates that the maximum ground surface settlement occurs at the location of 0.5H from the excavation edge. In addition, the ratio of the maximum ground surface settlement to the maximum lateral D-wall displacement ($\delta_{vmax}/\delta_{hmax}$) is 0.6.

2. The ground surface and adjacent building settlements are influenced by the 3D corner effect. The settlements around the corner of the excavation zone are about 20–50% of that occurs in the central section.

3. For the thick sand layer in Ho Chi Minh City, Vietnam, stiffness parameters E_{50} can be determined from the SPT-N value by the proposed formula $E_{50} = 2000N \times [1 + (0.0286z − 0.1429)^{0.5}]$. Note that the depth z should be in the range between 5 and 40 m.

4. The thick Ho Chi Minh sand layer should be divided into several layers for proper modeling by the HS soil model in FEA. The reference pressures P_{ref} is set to be equal to the minor effective principal stress σ'_3 at the middle of each layer while the E_{50}^{ref} should be determined from the average of SPT-N value in each layer.

5. The tilt of adjacent buildings is varied with the shape of ground deformation in each stage. The change of tilt depends on the length and the location of the adjacent building in the influence zone of the ground surface settlements.

6. The 2D simulations can be used to predict the damage degrees of the adjacent building at the initial design stages as well as the construction stages of the deep excavation work by determining the angular distortion β and the lateral strain ε_L from the FEA.
7. The damage potential of adjacent buildings as evaluated from FEA through the strain state chart proposed by Boscardin and Cording (1989) or the damage potential index (DPI) proposed by Schuster et al. (2009) is fairly accurate with field observations.

7 Notations

EA	axial stiffness
b	excavation width
c	adhesion factor
c_u	undrained adhesion factor
DPI	damage potential index
EI	flexural stiffness
E_{50}	secant stiffness at pressure level σ_3
E_{50}^{ref}	oedometer loading stiffness at a reference stress level p_{ref}
E_{oed}^{ref}	oedometer loading stiffness at a reference stress level p_{ref}
E_{ur}^{ref}	triaxial unloading stiffness at a reference stress level p_{ref}
H	excavation depth
L	excavation length
L_a	length of fixed-end anchor in the Plaxis model
$L_{spacing}$	spacing of anchor in Plaxis 2D model
m	power
SPT-N	SPT value
P_{ref}	preference pressure corresponding to E_{50}^{ref}
S_u	undrained shear strength
w	weight of the plate element
z	depth
β	angular distortion of the adjacent building
ε_L	lateral strain of the adjacent building
ε_p	principal strain of adjacent building
θ_{max}	direction of crack formation measured from the vertical plan
Δ_y	corresponding displacement of the fixed-end anchor of opening slabs
ν	Poisson's ratio
σ'_3	minor effective principal stress of layer soil
δ_{vm}	maximum settlement of ground surface
φ	internal friction angle
φ'	drained internal friction angle
φ_u	undrained internal friction angle

Authors' Contributions   Quoc Thien Huynh acquired methodology and software and contributed to the investigation.

Van Qui Lai acquired methodology, supervision, and contributed to conceptualization and writing—original draft.

Suraparb Keawsawasvong provided resources and contributed to writing—review and editing, data curation.

Tirawat Boonyatee provided resources and contributed to writing—review and editing, data curation.Data AvailabilityThe data and materials in this paper are available.

Compliance with Ethical Standards

Conflict of Interest   The authors declare that they have no conflict of interest.

References

AIJ. Recommendations for design of building foundations, AIJ 2001

Alshibli, K.A., Alsaleh, M.I.: Characterizing surface roughness and shape of sands using digital microscopy. J. Comput. Civ. Eng. **18**(1), 36–45 (2004)

Altun, S., Göktepe, B., Sezer, A.: Relationships between shape characteristics and shear strength of sands. Soils Found. **51**(5), 857–871 (2011)

Arai, K., Ohta, H., Kojima, K., WAKASUGI, M.: Application of back-analysis to several test embankments on soft clay deposits. Soils Found. **26**(2), 60–72 (1986)

Bjerrum, L.: Allowable settlement of structures. In: Proceedings of the 3rd European Conference on Soil Mechanics and Foundation Engineering. Wiesbaden, Germany (1963)

Boscardin, M.D., Cording, E.J.: Building response to excavation-induced settlement. J. Geotech. Eng. **115**(1), 1–21 (1989)

Burland, J.: "Behaviour of foundations and structures on soft ground." Proc. 9th ICSMFE, 1977, vol. 2, pp. 495–546 (1977)

Burland, J. B., Broms, B. B. and de Mello, V. F. 1978. "Behaviour of Foundations and Structures."

Clough, G.W.: Construction induced movements of in situ walls. In: Design and performance of earth retaining structures, pp. 439–470 (1990)

Cording, E., Long, J., Son, M., Laefer, D. and Ghahreman, B.. Assessment of excavation-induced building damage. Earth Retention Conference 3 (2010)

Finno, R.J., Calvello, M.: Supported excavations: observational method and inverse modeling. J. Geotech. Geoenviron. **131**(7), 826–836 (2005)

Gens, A., Ledesma, A., Alonso, E.: Estimation of parameters in geotechnical backanalysis—II. Application to a tunnel excavation problem. Comput. Geotech. **18**(1), 29–46 (1996)

Halim, D., Wong, K.S.: Prediction of frame structure damage resulting from deep excavation. J. Geotech. Geoenviron. **138**(12), 1530–1536 (2011)

Hsieh, P.-G., Ou, C.-Y.: Shape of ground surface settlement profiles caused by excavation. Can. Geotech. J. **35**(6), 1004–1017 (1998)

Hsiung, B.-C.B.: A case study on the behaviour of a deep excavation in sand. Comput. Geotech. **36**(4), 665–675 (2009)

Hsiung, B.-C.B., Dao, S.-D.: Evaluation of constitutive soil models for predicting movements caused by a deep excavation in sands. Electron. J. Geotech. Eng. **19**, 17325–17344 (2014)

Hsiung, B.-C.B., Yang, K.-H., Aila, W., Hung, C.: Three-dimensional effects of a deep excavation on wall deflections in loose to medium dense sands. Comput. Geotech. **80**, 138–151 (2016)

Hung, N.K., Phienwej, N.: Practice and experience in deep excavations in soft soil of Ho Chi Minh City, Vietnam. KSCE J. Civ. Eng. **20**(6), 2221–2234 (2016)

Huynh, Q.T., Lai V.Q., Tran, V.T., Nguyen, M.T.: Analyzing the settlement of adjacent buildings with shallow foundation based on the horizontal displacement of retaining wall. In: Geotechnics for Sustainable Infrastructure Development, pp. 313–320. Springer, Singapore (2020a)

Huynh, Q.T., Lai V.Q., Tran, V.T., Nguyen, M.T.: Back analysis on deep excavation in the thick sand layer by hardening soil small model. In: ICSCEA 2019, pp. 659–668. Springer, Singapore (2020b)

Khoiri, M., Ou, C.-Y.: Evaluation of deformation parameter for deep excavation in sand through case histories. Comput. Geotech. **47**, 57–67 (2013)

Likitlersuang, S., Plengsiri, P., Mase, L.Z., Tanapalungkorn, W.: Influence of spatial variability of ground on seismic response analysis: a case study of Bangkok subsoils. Bull. Eng. Geol. Environ. **79**(1), 39–51 (2020)

Likitlersuang, S., Surarak, C., Wanatowski, D., Oh, E., Balasubramaniam, A.: Finite element analysis of a deep excavation: a case study from the Bangkok MRT. Soils Found. **53**(5), 756–773 (2013)

Lim, A., Ou, C.-Y., Hsieh, P.-G.: Evaluation of clay constitutive models for analysis of deep excavation under undrained conditions. J. GeoEng. **5**(1), 9–20 (2010)

Lin, H.-D., Mendy, S., Liao, H.-C., Dang, P.H., Hsieh, Y.-M., Chen, C.-C.: Responses of 3D excavation and adjacent buildings in sagging and hogging zones using decoupled analysis method. J. GeoEng. **11**(2), 85–96 (2016)

Mana, A. I. and Clough, G. W.. "Prediction of movements for braced cuts in clay." Journal of Geotechnical and Geoenvironmental Engineering **107**(ASCE 16312 Proceeding) 1981

Mase, L.Z.: Liquefaction potential analysis along coastal area of Bengkulu Province due to the 2007 Mw 8.6 Bengkulu earthquake. Journal of Engineering and Technological Sciences. **49**(6), 721–736 (2017)

Misliniyati, R., Mase, L.Z., Irsyam, M., Hendriawan, H., Sahadewa, A.: Seismic response validation of simulated soil models to vertical array record during a strong earthquake. Journal of Engineering and Technological Sciences. **51**(6), 772–790 (2019)

Ou, C.-Y., Chiou, D.-C., Wu, T.-S.: Three-dimensional finite element analysis of deep excavations. J. Geotech. Eng. **122**(5), 337–345 (1996)

Ou, C.-Y., Hsieh, P.-G., Chiou, D.-C.: Characteristics of ground surface settlement during excavation. Can. Geotech. J. **30**(5), 758–767 (1993)

Ou, C. and Hsien, P. . Prediction of ground surface settlement induced by deep excavation, Geotechnical research report No. GT200008, Department of construction 2000

Plaxis 2D: Reference manual. Plaids BV, Amsterdam (2019)

Sabzi, Z., Fakher, A.: The performance of buildings adjacent to excavation supported by inclined struts. International Journal of Civil Engineering. **13**(1), 1–13 (2015)

Sadrekarimi, A., Olson, S.M.: Critical state friction angle of sands. Géotechnique. **61**(9), 771–783 (2011)

Sakurai, S., Akutagawa, S., Takeuchi, K., Shinji, M., Shimizu, N.: Back analysis for tunnel engineering as a modern observational method. Tunn. Undergr. Space Technol. **18**(2–3), 185–196 (2003)

Sakurai, S., Takeuchi, K.: Back analysis of measured displacements of tunnels. Rock Mech. Rock. Eng. **16**(3), 173–180 (1983)

Schanz, T., Vermeer, P., Bonnier, P.: The hardening soil model: formulation and verification. In: Beyond 2000 in computational geotechnics, pp. 281–296 (1999)

Schuster, M., Kung, G.T.-C., Juang, C.H., Hashash, Y.M.: Simplified model for evaluating damage potential of buildings adjacent to a braced excavation. J. Geotech. Geoenviron. **135**(12), 1823–1835 (2009)

Schweiger, H.. Influence of constitutive model and EC7 design approach in FEM analysis of deep excavations. Proceeding of ISSMGE International Seminar on Deep Excavations and Retaining Structures, Budapest (2009)

Shukor, F.: Comparison of back analysis and measured lateral displacement of cantilever diaphragm wall. Universiti Teknologi Malaysia, Johor Bahru (2009)

Skempton, A.W., MacDonald, D.H.: The allowable settlements of buildings. Proc. Inst. Civ. Eng. **5**(6), 727–768 (1956)

Son, M., Cording, E.J.: Estimation of building damage due to excavation-induced ground movements. J. Geotech. Geoenviron. **131**(2), 162–177 (2005)

Stroud, M.. "The standard penetration test: its application and interpretation." Penetration Testing in the UK: 29–49 (1989)

Tan, Y. and Chow, C. Design of retaining wall and support systems for deep basement construction–a Malaysian experience. Seminar on "Deep Excavation and Retaining Walls", Jointly orgnaised by IEM-HKIE, Malaysia (2008)

Teo, P., Wong, K.: Application of the hardening soil model in deep excavation analysis. The IES Journal Part A: Civil & Structural Engineering. **5**(3), 152–165 (2012)

Yong, C.C., Oh, E.: Modelling ground response for deep excavation in soft ground. Int. J. **11**(26), 2633–2642 (2016)

Zhang, R., Goh, A., Zhang, W.: System reliability assessment on deep braced excavation adjacent to an existing upper slope in mountainous terrain: a case study. SN Applied Sciences. **1**(8), 876 (2019)

Zhang, W., Goh, A.T., Zhang, Y.: Updating soil parameters using spreadsheet method for predicting wall deflections in braced excavations. Geotech. Geol. Eng. **33**(6), 1489–1498 (2015)

Zhang, W., Li, Y., Goh, A., Zhang, R.: Numerical study of the performance of jet grout piles for braced excavations in soft clay. Comput. Geotech. **124**, 103631 (2020)

Zhang, W., Zhang, R., Goh, A.T.: Multivariate adaptive regression splines approach to estimate lateral wall deflection profiles caused by braced excavations in clays. Geotech. Geol. Eng. **36**(2), 1349–1363 (2018a)

Zhang, X., Yang, J., Zhang, Y., Gao, Y.: Cause investigation of damages in existing building adjacent to foundation pit in construction. Eng. Fail. Anal. **83**, 117–124 (2018b)

Affiliations

Quoc Thien Huynh [1] · Van Qui Lai [2,3] · Tirawat Boonyatee [4] · Suraparb Keawsawasvong [5]

[1]   Institute of Research and Development, Duy Tan University, Danang 550000, Vietnam

[2]   Faculty of Civil Engineering, Ho Chi Minh City University of Technology, (HCMUT), 268 Ly Thuong Kiet Street, District 10, Ho Chi Minh City, Vietnam

[3]   Vietnam National University Ho Chi Minh City (VNU-HCM), Linh Trung Ward, Thu Duc District, Ho Chi Minh City, Vietnam

[4]   Department of Civil Engineering, Chulalongkorn University, Bangkok, Thailand

[5]   Department of Civil Engineering, Thammasat School of Engineering, Thammasat University, Pathumthani, Thailand